Gas-phase synthesis of magnesium nanoparticles

Kooi, B. J.; Palasantzas, G.; de Hosson, J. Th. M.

Published in:
Applied Physics Letters

DOI:
10.1063/1.2358860

Publication date:
2006

Gas-phase synthesis of magnesium nanoparticles: A high-resolution transmission electron microscopy study

B. J. Kooi, G. Palasantzas,[a] and J. Th. M. De Hosson
Department of Applied Physics, University of Groningen, Nijenborgh 4, 9747 AG Groningen, The Netherlands; The Netherlands Institute for Metals Research, University of Groningen, Nijenborgh 4, 9747 AG Groningen, The Netherlands; and Materials Science Center, University of Groningen, Nijenborgh 4, 9747 AG Groningen, The Netherlands

(Received 18 May 2006; accepted 16 August 2006; published online 19 October 2006)

Magnesium nanoparticles with size above 10 nm, prepared by gas-phase syntheses, were investigated by high-resolution transmission electron microscopy. The dominant particle shape is a hexagonal prism terminated by Mg(0002) and Mg$\{10\bar{1}0\}$ facets. Oxidation of Mg yields a MgO shell (~3 nm thick), which has an orientation relation with the Mg. Inhomogeneous facet oxidation influences their growth kinetics resulting in a relatively broad size and shape distribution. Faceted voids between Mg and MgO shells indicate a fast outward diffusion of Mg and vacancy rearrangement into voids. The faceting of polar {220} planes is assisted by electron irradiation. © *2006 American Institute of Physics*. [DOI: 10.1063/1.2358860]

In recent years, magnesium has attracted strong interest as possible high performance hydrogen storage material.[1–9] Because the storage capacity is limited by material weight, significant attention has been paid to lightweight materials.[3–9] In addition from fundamental point of view, Mg is an instructive case to explore the transition from nonmetallic-to-metallic behavior because its electronic structure varies dramatically with the number of interacting atoms.[10] The *s-p* band gaps were observed to close at 18 atoms (particle sizes >0.9 nm), signaling the onset of metallic behavior and giving a possible lower limit to sizes for storage applications.[11]

The kinetics of H absorption/desorption and the heat release during hydrogenation can be tailored by refining the size of the nanoparticle. Calculations have shown that as the particle size increases from 0.6 to 2 nm, the heat of formation increases from 16 to 19 kcal/Mg and approaches the bulk value (~20.00 kcal/Mg) beyond 2 nm.[12] Studies of Mg powders showed that their chemical reactivities were approximately proportional to their specific surface areas for particle sizes down to 76 nm.[13] The pressure plateau, at which the material reversibly absorbs/desorbs hydrogen, is of primary importance for storage by metal hydrides. Studies of nanoparticle (e.g., Pt and Pd) assemblies have also shown the absence of a pressure plateau for sizes <3 nm.[14]

Previous work has addressed the effect of oxidation on the hydrogen uptake in 400 nm thick Mg films.[15] Oxygen initially increased the hydrogen uptake rate, which was decreased at higher oxygen concentrations due to the formation of MgO layers. It is also likely that the formation of an ultrathin MgO layer can favor hydrogen diffusion into the bulk of Mg by prohibiting the formation of surface MgH_2 that further frustrates hydrogen diffusion.[15] Therefore, understanding structural aspects of Mg nanoparticles with size larger than 1 nm is important for future applications of complex nanostructured Mg-based hydrogen storage systems. So far, little is known about the effect of the oxidation on the structure evolution of gas-phase synthesis of Mg nanoparticles. Here, we will investigate these issues using high-resolution transmission electron microscopy (HRTEM).

The chamber of the nanoparticle (NC200U) source was evacuated to a base pressure of $\sim 3\times 10^{-9}$ mbar with partial oxygen pressure in $\sim 10^{-10}$ mbar range. Supersaturated metal vapor is generated by sputtering a Mg target (purity of 99.95% as obtained by Alfa Aesar) in an inert gas atmosphere of Ar (pressure of ~0.4 mbar).[16,17] Particles were removed fast from the aggregation zone by the use of He as a drift gas. HRTEM imaging and electron diffraction analysis were performed using a JEOL 2010F, with the nanoparticles deposited on commercial amorphous silicon-nitride membranes of 25 nm thick.[16,17]

Figures 1–3 demonstrate a variety of two dimensional TEM projections of nanoparticles. About 80% Mg particles show a hexagonal shape (or where adjacent facets in projection make mutual angles of 120°). The diffraction pattern [Fig. 2(b)] shows that imaging in this case occurred along the (hcp) Mg[0001] direction, and the observed facets for this projection are Mg$[10\bar{1}0]$. The second most abundant particle orientation with respect to the substrate (~1 in 8) is shown

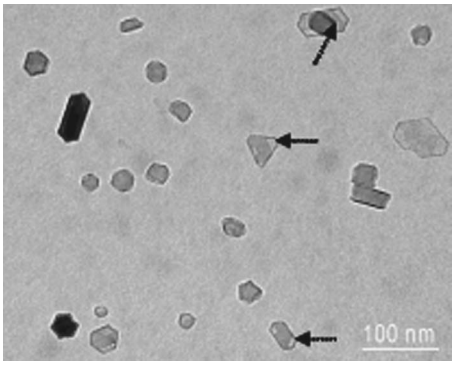

FIG. 1. Bright-field TEM image showing Mg nanoparticles with various orientations with respect to the substrate. Most Mg particles are viewed near to [0001] and show $\{10\bar{1}0\}$ facets with mutual angles of 120°. A significant number of particles show hollow internal parts between Mg core and MgO shell as indicated by the arrows.

[a]Author to whom correspondence should be addressed; electronic mail: g.palasantzas@rug.nl

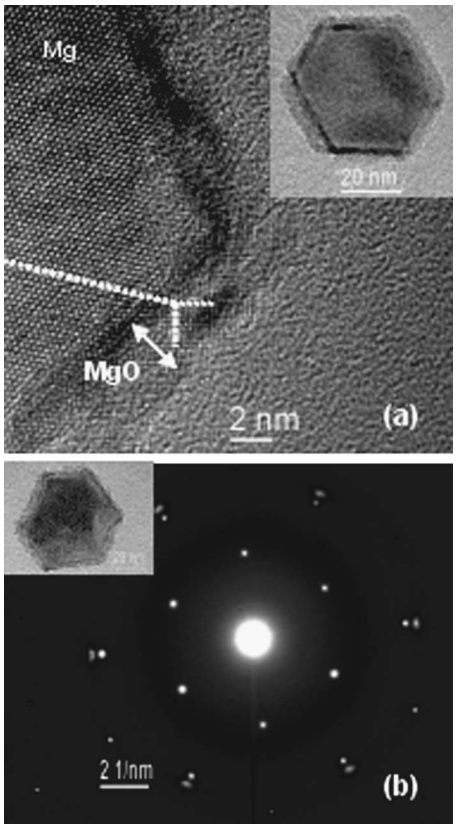

FIG. 2. (a) HRTEM image where Mg core and MgO shell crystal structure are simultaneously resolved. The Mg is viewed along [0001] and the MgO along [001] directions. The inset shows the hexagonal nanoparticle. (b) Electron diffraction pattern for the Mg cluster shown in the inset.

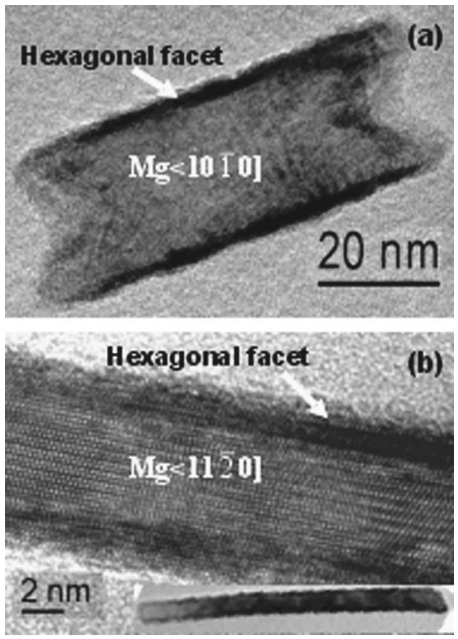

FIG. 3. (a) Mg nanoparticle viewed along $\langle 10\bar{1}0\rangle$. Similar particle type as in Fig. 2(a) and as most frequently observed in Fig. 1, but taken under 90° angle. (b) HRTEM image of needle-shape Mg nanoparticle (inset: full shape of ~80 nm in length) as viewed along $\langle 11\bar{2}0\rangle$.

in Fig. 3(a), which yields a needle shape two dimensional particle projection. It corresponds to the same three-dimensional shape but projected in a direction perpendicular to the [0001], namely, $\langle 10\bar{1}0\rangle$. For this projection and particle type it is clear that the stable facet is the Mg(0002). The Mg[0001] and $\langle 10\bar{1}0\rangle$ projections indicate the hexagonal prism as the most stable shape of the Mg particles. The stable shape of the particles is determined by surface energies (which can be derived by the Wulff construction[18]), where the facets correspond to the closest packed planes. More interestingly, since 80% of the particles have their Mg[0001] direction perpendicular to the plane of the membrane, it can be concluded that they can attain energetically favorable orientations, controlled by interface energies, upon soft landing. Thus, the nanoparticles can rotate themselves towards a more favorable orientation upon landing on the substrate.

Factors such as temperature, kinetics, impurities, and surface energies can lead to unusual nanoparticle shapes and size distributions.[18] Comparison of Mg particles with other nanoparticles we studied earlier, Cu, Co, Fe, Nb, and Mo[17] shows that their size distribution is significantly broader. Crucial is the oxide shell formation around the particles. Nonuniform oxidation of various particle facets is the origin of the broader size and shape distribution. The HRTEM image in Fig. 2(a) confirms the formation of a thin fcc MgO shell (~3 nm thick). For Fe nanoparticles the oxide shell of similar thickness was amorphous and developed during sample transfer to TEM.[19] In contrast, the MgO shell forms within the deposition chamber during particle growth, since particles that directly after deposition were covered with a Ti film showed identical MgO shells. The MgO shell prevents further oxidation under ambient conditions since the shells were the same for freshly deposited and samples kept for one month in air. The oxidation of Mg also leads to the formation of sharply faceted voids [arrows in Fig. 1(b)] since the outward diffusion of Mg is faster than inward diffusion of O to form MgO. The large hollow voids are also formed due to fast vacancy clustering, and they are more susceptible to electron beam damage [comparing Figs. 4(c) and 4(a)].

In general, at room temperature (RT) dense oxide films on metals exhibit a limiting thickness of a few nanometers as explained by the coupled currents approach of Fromhold and Cook.[20] In this case, outward diffusion of cations or inward diffusion of anions, which is needed for oxide growth, has to be balanced by transport of electrons from the metal-oxide interface to the oxide surface where ionization of the adsorbed oxygen occurs. At lower temperatures, e.g., at RT, electron transport through the dense oxide film is only possible by a (single step) tunneling mechanism. Since the latter decreases exponentially with increasing layer thickness, oxide growth stops after a few nanometers if no other electron transport mechanisms (e.g., thermionic emission) are sufficiently active.[20] This explain the formation of the relatively uniform MgO thickness that is stable in time preventing further oxidation.

The selected area electron diffraction (SAED) pattern in Fig. 2(b) in combination with HRTEM images yields the orientation relation (OR) between Mg and MgO. Many images show that the Mg$\{10\bar{1}0\}$ facets, as viewed along Mg[0001], are parallel to MgO{220} as viewed along MgO[001] [Fig. 2(a)]. The MgO(200) and (020) planes are resolved in Fig. 2(a). Due to limited thickness of MgO (~2–3 nm), when viewing along MgO[001], the (200), (020), and the (220) reflections (the latter corresponds to planes parallel to the Mg facet) are not observable in the SAED patterns. The $(2\bar{2}0)$ reflection is observable and cor-

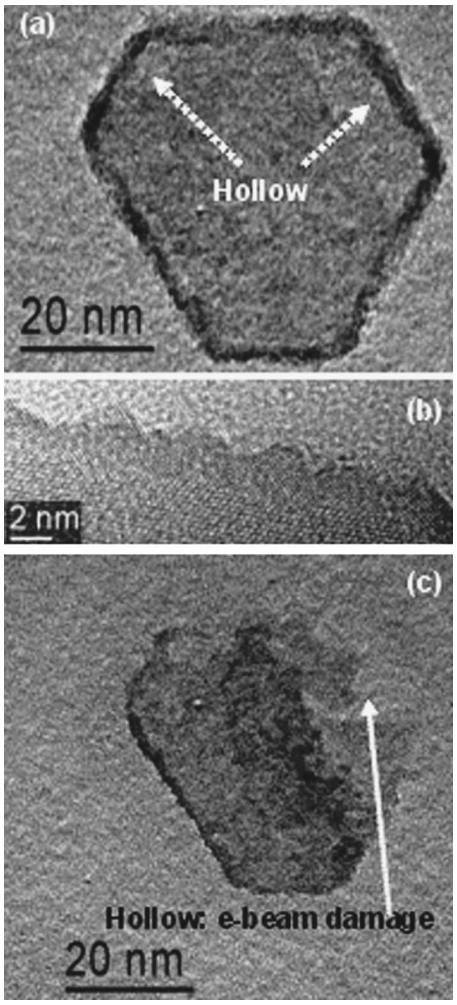

FIG. 4. (a) TEM image of an Mg particle viewed along [0001] with faceted hollow parts as indicated by the arrows. (b) HRTEM image of an MgO shell around the Mg, where faceting of the original Mg(220) surface into MgO(200) and (020) surfaces has taken place. (c) TEM image of the same nanoparticle as in (a) after prolonged exposure to the electron beam leading to damage around the hollow area.

responds to planes perpendicular to the Mg$(10\bar{1}0)$ facet. Therefore, the OR for these facets is Mg[0001]‖MgO[001] and Mg$(10\bar{1}0)$‖MgO(220). This implies that at the corners of the adjacent Mg$\{10\bar{1}0\}$ facets (making mutual angles of 120°), the MgO on these two facets show a mutual misorientation of 30°. Also an OR exists between the MgO and Mg on the Mg(0002) facets as shown in Fig. 3(a) with Mg$(11\bar{2}0)$‖MgO[220] or Mg$(1\bar{1}00)$‖MgO$[2\bar{2}0]$ and Mg(0002)‖MgO(002). This means that the MgO on the pair of Mg(0002) facets has the same orientation as on one of the three pairs of Mg$\{10\bar{1}0\}$ facets. To the best of our knowledge, this OR is observed for the first time for MgO/Mg nanoparticles interfaces. The main reason for this OR originates from a most dense packing at the metal-oxide interface providing a large number of metal-oxygen bonds to be established across the interface.[21]

It is noteworthy that the polar (220) surface of MgO shows a reconstruction, which is aided by the electron beam [Fig. 4(b)]. The lateral size of the facet is between a few atomic steps up to ~3 nm, which is comparable to the MgO thickness. The MgO(200) surface has the lowest surface energy in ionic rocksalt materials, while other facets such as Mg(111) and MgO(220) are unstable polar surfaces in vacuum. The latter lower their energy by surface (geometrical/electronic) reconstruction, faceting, and adsorbates.[22]

In conclusion, Mg nanoparticles with sizes in between 10 and 80 nm produced by gas-phase synthesis have a hcp structure with a hexagonally prismatic shape. Deviations from this shape and the relatively broad particle size distribution are attributed to the oxidation of Mg. The oxidation leads to hollow sharply faceted voids at the Mg/MgO interface. The latter is due to faster outward diffusion of Mg compared to inward diffusion of oxygen, and fast rearrangement of vacancies to form faceted voids. The crystalline MgO shell (~3 nm) shows an orientation relation with Mg, and undergoes faceting (with size ⩽3 nm) assisted by electron beam irradiation to stabilize polar {220} MgO surfaces.

The authors would like to thank the MSC for support.

[1] E. Akiba, Curr. Opin. Solid State Mater. Sci. **4**, 267 (1999).
[2] G. Sandrock, J. Alloys Compd. **293**, 877 (1999).
[3] L. Schlapbach and A. Züttel, Nature (London) **414**, 353 (2001).
[4] W. Grochala and P. Edwards, Chem. Rev. (Washington, D.C.) **104**, 1283 (2004).
[5] F. Schüth, B. Bogdanoviæ, and M. Felderhoff, Chem. Commun. (Cambridge) **2004**, 2249.
[6] A. C. Dillon, K. M. Jones, T. A. Bekkedahl, C. H. Kiang, D. S. Bethune, and M. J. Heben, Nature (London) **386**, 377 (1997).
[7] P. Chen, X. Wu, J. Lin, and K. L. Tan, Science **285**, 91 (1999).
[8] S. Orimo, G. Majer, T. Fukunaga, A. Züttel, and L. Schlapbach, Appl. Phys. Lett. **75**, 3093 (1999).
[9] P. Chen, Z. Xiong, J. Luo, J. Lin, and K. L. Tan, Nature (London) **420**, 302 (2002).
[10] O. C. Thomas, W. Zheng, S. Xu, and K. H. Bowen, Jr., Phys. Rev. Lett. **89**, 213403 (2002); P. H. Acioli and J. Jellinek, *ibid.* **89**, 213402 (2002); J. Jellinek and P. H. Acioli, J. Phys. Chem. A **106**, 10919 (2002).
[11] R. W. P. Wagemans, J. H. van Lenthe, P. E. de Jongh, A. J. van Dillen, and K. P. de Jong, J. Am. Chem. Soc. **127**, 16675 (2005).
[12] S. Cheung, W.-Q. Deng, A. C. T. van Duin, and W. A. Goddard III, J. Phys. Chem. A **109**, 851 (2005).
[13] Y. Zhang, S. Liao, Y. Fan, J. Xu, and F. Wang, J. Nanopart. Res. **3**, 23 (2001).
[14] H. Goto and T. Furata, Published online at http://www.h-workshop.uni-konstanz.de/talks.html, H-workshop 2005, http://www.h-workshop.uni-konstanz.de/, Physics Center Bad Honnef, Germany, 23–28 October 2005.
[15] P. Hjort, A. Krozer, and B. Kasemo, J. Alloys Compd. **237**, 74 (1996); J. Ryden, B. Hjörvarsson, T. Ericsson, E. Karlsson, A. Krozer, and B. Kasemo, J. Less-Common Met. **152**, 295 (1989).
[16] H. Haberland, M. Moseler, Y. Qiang, O. Rattunde, T. Reiners, and Y. Thurner, Surf. Rev. Lett. **3**, 887 (1996).
[17] G. Palasantzas, S. A. Koch, and J. Th. M. De Hosson, Appl. Phys. Lett. **81**, 1089 (2002); T. Vystavel, G. Palasantzas, S. A. Koch, and J. Th. M. De Hosson, *ibid.* **83**, 3909 (2003); S. A. Koch, R. H. te Velde, G. Palasantzas, and J. Th. M. De Hosson, *ibid.* **84**, 556 (2004); T. Vystavel, G. Palasantzas, S. A. Koch, and J. Th. M. De Hosson, *ibid.* **86**, 113113 (2005).
[18] *Nanomaterials: Synthesis, Properties and Applications*, edited by A. S. Edelstein and R. C. Cammarata (Institute of Physics, Bristol, 1998), Chap. 2, pp. 13–54.
[19] T. Vystavel, G. Palasantzas, S. A. Koch, and J. Th. M. De Hosson, Appl. Phys. Lett. **82**, 197 (2003).
[20] A. T. Fromhold, Jr. and E. L. Cook, Phys. Rev. **158**, 600 (1967); **163**, 650 (1967); A. T. Fromhold, Jr., *Theory of Metal Oxidation: Fundamentals* (North-Holland, Amsterdam, 1976), Vol. I.
[21] B. J. Kooi and J. Th. M. De Hosson, Acta Mater. **48**, 3687 (2000).
[22] C. Noguera, J. Phys.: Condens. Matter **12**, R367 (2000); C. Noguera, A. Pojani, P. Casek, and F. Finocchi, Surf. Sci. **507–510**, 245 (2002).